RESEARCH ARTICLE

National Science Open
2: 20230019, 2023
https://doi.org/10.1360/nso/20230019

Chemistry

Sustainable production of value-added *N*-heterocycles from biomass-derived carbohydrates via spontaneous self-engineering

Feng Yu[1,2,*,#], Chong Liu[3,#], Fenghua Tan[4], Yuhe Liao[4], Liang Wang[2], Yuping Li[4] & Feng-Shou Xiao[1,2,*]

[1]*Key Lab of Applied Chemistry of Zhejiang Province, Department of Chemistry, Zhejiang University, Hangzhou 310028, China;*
[2]*Key Lab of Biomass Chemical Engineering of Ministry of Education, College of Chemical and Biological Engineering, Zhejiang University, Hangzhou 310027, China;*
[3]*State Key Laboratory of Structural Chemistry, Fujian Institute of Research on the Structure of Matter, Chinese Academy of Sciences, Fuzhou 350002, China;*
[4]*Guangzhou Institute of Energy Conversion, Chinese Academy of Sciences, Guangzhou 510640, China*

#Contributed equally to this work.

Received 20 March 2023; Revised 3 July 2023; Accepted 5 July 2023; Published online 1 November 2023

Abstract: Abstract: Synthetic *N*-heterocyclic compounds, such as quinoxalines, have shown a crucial role in pharmaceutical as well as food and dye industries. However, the traditional synthesis toward *N*-heterocycles relies on multistep energy and cost-intensive non-sustainable processes. Here, we report a facile approach that allows one-step conversion of biomass-derived carbohydrates to valuable quinoxalines in the presence of aryl-1,2-diamines in water without any harmful metal catalysts/organic solvents via spontaneously engineering involved cascade reactions under hydrothermal conditions. Aryl-1,2-diamines are revealed as the key to propel this transformation through boosting carbohydrate fragmentation into small 1,2-dicarbonyl intermediates and subsequently trapping them for constituting stable quinoxaline scaffolds therefore avoiding a myriad of undesired side reactions. The tunability of product selectivity can be also achievable by adjusting the basicity of the reaction environment. Both batch and continuous-flow integrated processes were verified for production of quinoxalines in an exceptionally eco-benign manner (*E*-factor <1), showing superior sustainability and economic viability.

Keywords: Keywords: biomass conversion, sustainability, green chemistry, carbohydrate, *N*-heterocycle

INTRODUCTION

With the diminishment of petroleum resources and rise of carbon footprint, there is an urgent need to discover and implement greener chemical transformations for the production of chemicals, which should preferably utilize lignocellulosic biomass, the largely abundant and cheap renewable carbon source on the earth, as feedstock, operate in a simple and economical way, use green solvent and make no hazardous waste at all, to replace current petroleum-based chemical manufacturing processes [1–12]. Thus, exploring sustainable and efficient synthetic approaches, especially with simply operational and green features, for converting lignocellulosic resources (e.g., carbohydrates) into high-value yet challenging *N*-heterocyclic chemicals is growing to be of significant importance [13–15].

Quinoxalines are an important class of *N*-heterocycles, which are crucial structural scaffolds found in a

diverse library of therapeutically useful agents in medicinal chemistry, and their derivatives are also widely used as dyes, food additives, pharmaceuticals [16,17]. Currently, the prevalent route for production of quinoxalines is through condensation of aryl-1,2-diamines with 1,2-dicarbonyls [18]. For instance, the condensation of pyruvaldehyde (PA) with *o*-phenylenediamine (*o*-PDA) yields 2-methylquinoxaline, which is widely used as a flavoring ingredient in food industry [19] and served as a valuable building block for synthesizing a wide spectrum of antibiotics and antifungal drugs [20,21]. Nevertheless, high operation cost in the production and purification of PA, via regardless of enzymatic or chemical processes, largely affects the feasibility of the synthetic process in practical production as well as the market price of quinoxalines. Today chemical production of PA mainly relies on traditional petroleum-based routes starting from propane, which include propylene glycol and acetone routes (Figure 1A). The propylene glycol route (Route 1) involves the formation of propylene oxide intermediate through chlorohydrin technology and subsequent hydrolysis to generate propylene glycol, which is followed by oxidation at high temperature [22–24]. The acetone route (Route 2) involves the transformation of propene to acetone via the classical cumene process and a subsequent oxidation reaction [25,26]. Both routes to PA necessitate several reaction steps and the purification operations for each-step product as well as the use of harmful metal catalysts/organic solvents, eventually resulting in low overall efficiencies but high operation cost and environmental pollution.

In the hydrothermal degradation of carbohydrates, 1,2-dicarbonyls (e.g., PA) are observed as the important intermediates [27]. However, they are more prone to forming humin by-products because of their high reactivity rendered by carbonyl groups [28], consequently lowering the efficiency of the biorefinery process. *In-situ* trapping of these valuable yet transient 1,2-dicarbonyl intermediates towards fabricating desired compounds could be a solution to improving the efficiency of carbohydrate utilization, but unfortunately it has long been overlooked. Recently, alkylamines with NH_2 or NH groups were found to be able to sub-

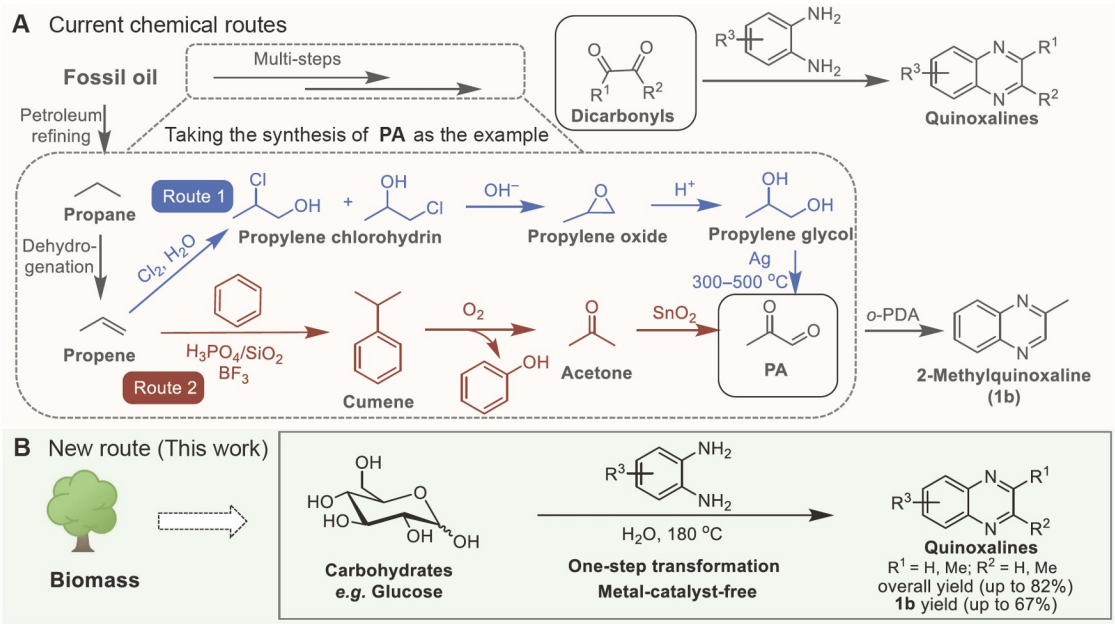

Figure 1 Current and proposed chemical approaches for manufacturing quinoxalines. (A) Currently primary petroleum-based routes (Routes 1 and 2 are exemplified for the production of PA and corresponding 2-methylquinoxaline). (B) Our proposed one-step sustainable approach based on biomass-derived carbohydrates.

stantially facilitate sugar fragmentation via aldolase-like Retro-Aldol means [29,30]. Inspired by this finding and the above-mentioned in-situ 1,2-dicarbonyls-trapping concept, we envisage that if aryl-1,2-diamines, possessing both primary amino group and excellent 1,2-dicarbonyl trapping capability for quinoxaline skeleton fabrication, are introduced into the sugar transformation under hydrothermal conditions, one-step conversion of sugars to desirable quinoxalines may be achievable (Figure 1B). Importantly, with this transition-metal-free strategy, intractable side reactions arising from highly active 1,2-dicarbonyl species, pervasive in sugar degradation, could be considerably inhibited, and the reaction efficiency could be improved significantly.

RESULTS

Optimization of the reaction

Considering that glucose is one of the most abundant and cheapest sugars on the earth, an initial attempt was made to assess the feasibility of the reaction for converting glucose into quinoxalines in presence of *o*-PDA in water at 150ºC under 2 MPa N_2. Pleasingly, after 5 h glucose was completely consumed in conjunction with the appearance of three quinoxalines, including quinoxaline (**1a**, 13%), 2-methylquinoxaline (**1b**, 33%), and 2,3-dimethylquinoxaline (**1c**, 6%) (Table 1, entry 1). The reaction was promoted at elevated temperature and capable of achieving the maximum overall yield of quinoxalines **1a**–**1c** (81%) at the temperature of 180ºC (Table 1, entries 2 and 3, and Table S2, entries 1–5). Reaction atmosphere showed minor impact on the transformation, while N_2 pressure effect was found to be negligible (Table 1, entry 2, and Table S3, entries 2 and 3). Attempts of introducing state-of-the-art homogeneous ($AlCl_3$/$SnCl_2$) [31] and solid (Sn-Beta) [27] catalysts, which allow efficient transformation of sugars into lactic acid (LA) via a PA route, to boost the reaction efficiency were proven to be failures (Table 1, entries 4 and 5). Specifically, the addition of homogeneous $AlCl_3$/$SnCl_2$ catalyst system into the reaction of glucose with *o*-PDA led to a substantial decrease in the reaction efficiency for the production of quinoxalines. This result may be due to the coordination effect between metal ions (Al^{3+}, Sn^{2+}) and *o*-PDA, which intercepts the interaction of glucose with *o*-PDA and accordingly impedes the reaction for quinoxalines production. The effect of a solid Sn-Beta catalyst on the reaction is negligible. The reaction with Sn-Beta gives almost same results when compared to that from the reaction in the absence of Sn-Beta. These results suggest that glucose transformation to quinoxalines is mainly dominated by *o*-PDA.

To reveal the significance of *o*-PDA in glucose degradation, glucose carbon distributions of reactions with different additives are presented (Figure 2A). Without additive, glucose degradation in H_2O at 180ºC under N_2 was rather difficult to proceed, merely affording little amounts of C_3 products (3%) after 5 h (Table S4). However, an addition of amine, either aniline or *o*-PDA, led to full glucose conversion (>99%) under identical conditions. In the reaction with aniline, a number of products including C_6, C_3, and C_2, were produced from glucose with very low yields (Table S4). Among these products, indole exhibited the highest yield of 6%. The reaction mixture seemed muddy and black (Figure S6), implying a low reaction efficiency, likely due to the formation of low-soluble complex by-products. By contrast, the addition of *o*-PDA provided a remarkable enhancement in reaction efficiency, yielding quinoxalines **1a** (19%), **1b** (50%), and **1c** (11%), which accounted for ⩾95% of all identified products in this reaction (Figures 2A and 2B). The introduction of

Table 1 Catalytic production of quinoxalines from carbohydrates and their derived feedstocks[a]

Entry	Carbohydrate or its derivative	Catalyst or additive	Temp. (°C)	Time (h)	Yield of quinoxalines (%)[b]			
					 **1a**	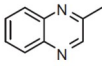 **1b**	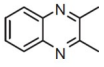 **1c**	Total
1	Glucose	–	150	5	13	33	6	52
2	Glucose	–	180	5	19	50 (46)	11	80
3	Glucose	–	120	18	7	19	2	28
4[c]	Glucose	$AlCl_3/SnCl_2$	180	4	18	12	7	37
5[d]	Glucose	Sn-Beta	180	5	19	51	11	81
6	Glucose	Na_2CO_3	180	5	3	55	5	63
7	Glucose	K_2CO_3	180	5	3	65	4	72
8	Glucose	LiOH	180	5	3	51	2	56
9	Glucose	NaOH	180	5	6	64	7	77
10	Glucose	KOH	180	5	6 [6]	66 [67] (64)	7 [6]	79
11	Glucose	$Ca(OH)_2$	180	5	8	65	4	77
12	Fructose	KOH	180	5	7	67	7	81
13	Mannose	KOH	180	5	6	65	8	79
14	Pyruvaldehyde	–	180	0.25	2	95	0	97
15	Glyceraldehyde	–	180	2	6	51	1	58
16	Dihydroxyacetone	–	180	2	5	85	0	90
17	Lactic acid	–	180	4	0	0	0	0

a: Reaction conditions: carbohydrate feedstock (0.5 mmol), *o*-PDA (2 mmol), H_2O (20 mL), N_2 (2 MPa). For the reactions with alkalis, 0.15 mmol alkali was employed except for $Ca(OH)_2$ (7.5×10^{-2} mmol instead). b: Yields are based on average value from duplicate experiments with error <2%, determined by gas chromatography (GC). Values in parentheses and brackets indicate the isolated and NMR yields, respectively. c: $AlCl_3$ and $SnCl_2$ (10 mol% each) were employed. d: Sn-Beta (3 mol%, based on Sn content) were employed. Mass balance is not complete due to undesired competitive reactions of the Maillard type and/or caramelization.

o-PDA led to the glucose degradation much more kinetically favorable, demonstrating a 108-fold increase in the degradation rate. It should be noted that the carbon balance of the glucose reaction by using aniline was estimated to be 17 C%, which is much lower than that (~80%) from the reaction of glucose with *o*-PDA, indicating the importance of the selection of amine in carbon utilization of glucose for manufacturing specific products. The slight carbon loss in the reaction of glucose in the presence of *o*-PDA was due to the undesired competitive side reactions of the Maillard type and/or caramelization [30,32–34], which are commonly observed in the reactions between sugars and amino-containing compounds.

In addition, the yield of **1b** was further increased to 66% in the presence of a minimal amount of base (Figure 2C and Table 1, entries 6–11), which is in line with the previous findings on base's ability of boosting glucose fragmentation into C_3 products [35–37]. Strong bases including NaOH, KOH, and $Ca(OH)_2$, gave ~65% yield of **1b** and around 77% overall yields of quinoxaline products, which are higher than the **1b** yield (55%) and the overall yield (63%) from the weak base Na_2CO_3, indicating a positive effect of high basicity on the reaction efficiency. A particularly low yield (51%) of **1b** with strong base LiOH and a relatively high **1b** yield (65%) obtained in the case of using weak base K_2CO_3 suggest that in addition to the basicity of the base, its cation could also bring an impact on the reaction. It should be noted that the use of a base, though in a small quantity, for chemical production would usually cause basic waste water treatment issues, which not only increases the complexity of production processes, but also enhances the economic and environmental cost. However, in the case of our proposed reaction, a neutralization treatment for the resulted waste water is not needed because the acidic byproducts such as LA, glycolic acid (GLA), formic acid (FA), and Maillard

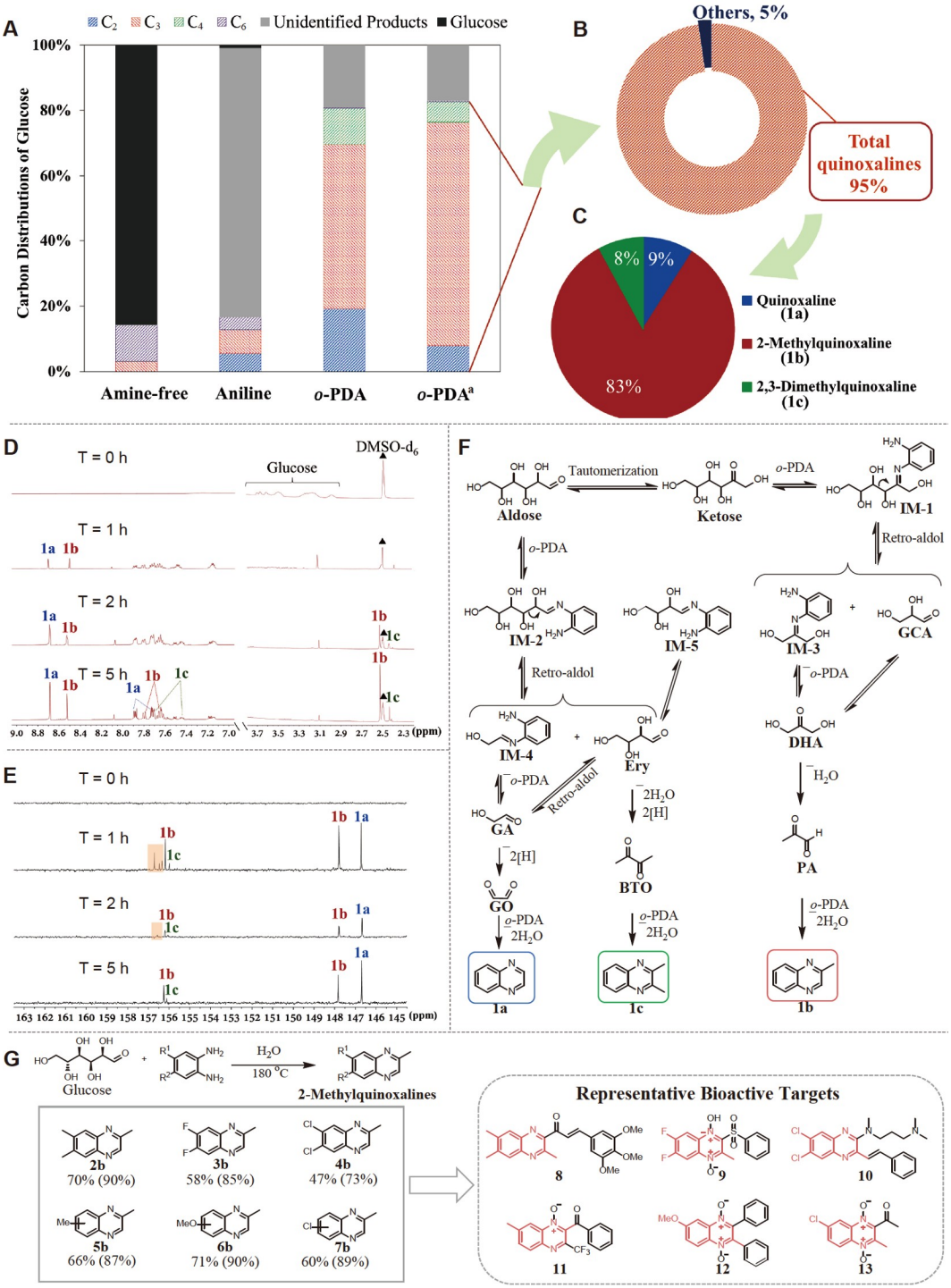

Figure 2 Transformation of glucose to quinoxalines. (A) Carbon distributions of glucose for the reaction with different additive. Reaction conditions: glucose (0.5 mmol), H_2O (20 mL), 180ºC, 5 h, N_2 (2 MPa), the amount of amine additive (aniline and *o*-PDA) was based on total amino groups (4 mmol). [a] KOH (0.15 mmol) was added. (B) The composition of identified products obtained from glucose transformation in the presence of *o*-PDA and KOH. (C) The composition of total formed quinoxalines. The reaction progression monitored by ^{1}H NMR (D) and ^{13}C NMR (E). (F) Proposed plausible reaction pathways for transforming glucose into quinoxalines in the presence of *o*-PDA. Cyclic forms of the sugars are omitted for clarity. (G) Synthesis of various 2-methylquinoxalines via the proposed reaction with a minimal KOH additive and their potential for manufacturing high-value bioactive compounds. The values in the parentheses indicate the percentage of the corresponding 2-methylquinoxalines in total formed quinoxaline products.

type-derived oligomeric/polymeric molecules, generated during the reaction have self-neutralized the initially added base, indicating the use of base in the presented reactions would not cause extra environmental burden.

Fructose, a ketose favorably cleaved into two C_3 fractions [38], did not show a significant effect on **1b** yield (67%) (Table 1, entry 12), likely due to a rapid equilibrium reached between ketoses and aldoses via tautomerization under reaction conditions [39]. This is supported by similar results (65% yield) obtained in the reaction of mannose (Table 1, entry 13). In addition, several C_3 feedstocks, including glyceraldehyde (GCA), dihydroxyacetone (DHA), PA, and LA, which are typical products from glucose hydrothermal degradation, were also investigated to gain insights into the reaction pathways. Among all C_3 feedstocks, PA exhibited best performance in both reaction rate and product yield, giving 95% yield of **1b** and 2% yield of **1a** in only 15 min (Table 1, entry 14). DHA exhibited higher efficiency in **1b** production than GCA (Table 1, entries 15 and 16). It should be noted that product **1a** can be slowly generated from GCA, DHA, and PA with prolonging time. In addition to **1a**, a minimal amount of **1c** (~1%) was also detected in the GCA transformation after 4 h, implying C_3-to-C_2 and C_3-to-C_4 transformations are able to occur via aldol and retro-aldol reactions [40]. No quinoxalines were obtained from LA (Table 1, entry 17), ruling out the possibility that LA was involved in the formation of **1a**–**1c**.

Mechanistic insights into the reaction pathways

Monitoring the glucose reaction with *o*-PDA at specific temperature by nuclear magnetic resonance (^{1}H and ^{13}C NMR) and liquid chromatography-mass spectrometry (LC-MS) technologies were performed (Figures 2D and 2E, and Figures S12–S15). The kinetic profiles at temperatures of 140, 180, and 190°C (Figure S12) showed that glucose was fast consumed in the initial stage upon the interaction with *o*-PDA. With the glucose conversion, fructose was rapidly formed and gradually consumed after passing the maximum yield (36%–40%). With time, quinoxalines **1a**–**1c** were progressively produced as the main products and ultimately achieved steady yields. These reaction time course profiles clearly indicate that fructose acts as an important intermediate in the reaction of converting glucose to quinoxalines. Increasing the temperature could significantly accelerate the reaction rate, which consequently shortens the time duration required for reaction completion from 12 h at 140°C to only 4 h at 190°C. Additionally, the beneficial effect of increased temperature on production of quinoxalines was also observed, improving the overall yield of quinoxalines **1a**–**1c** from 66% at 140°C to 81% at 190°C. For the reactions in the presence of a small quantity of KOH, **1b** presented as the main product (Figure S16). The appearance of peaks at around 156 ppm in the ^{13}C NMR spectrum after 1 h and their subsequent disappearance with time suggest imine intermediates may be involved in the reaction (Figure 2E), likely through iminization of *o*-PDA with carbonyl-functionalized substrates, such as C_6 sugars and their derived fragments. The generation of imines is consistent with the typical pathways for amine-facilitated glucose fragmentation [29,30] and amine-participated Maillard type reactions [32], which is further supported by the detection of corresponding *m*/*z* by electro spray ionization mass (ESI-MS, Figure S15). Based on these results, we propose the plausible reaction pathways depicted in Figure 2F.

The proposed pathways start with sugar isomerization and rapidly achieve an equilibrium between ketoses and aldoses. The nucleophilic attack of the NH_2 group of *o*-PDA on carbonyl group of sugars allows the iminization to take place on both ketose and aldose, leading to IM-1 and IM-2 respectively. IM-1 then

undergoes an amine-facilitated retro-aldol reaction, resulting in the formation of IM-3 and GCA via cleaving C3–C4 bond. DHA can be generated from IM-3 via hydrolysis or from GCA via isomerization. The formed trioses including DHA and GCA are susceptible to dehydration to produce reactive PA, which is rapidly trapped by *o*-PDA and cyclized to form the desired product **1b**, therefore preventing its further hydration into LA and other by-products formation [35]. Meanwhile, a competitive C2–C3 cleavage of aldose also occurs via an analogical route involving glyoxal (GO) and butanedione (BTO) intermediates as previously reported in amino acid-facilitated Maillard reaction [41,42], eventually giving rise to products **1a** and **1c**. Specifically, a retro-aldol reaction of aldose-derived IM-2 results in its C2–C3 cleavage and gives rise to the formation of smaller sugars including GA and Ery, which are further subjected to the redox reactions, leading to the formation of GO and BTO, respectively. The formed dicarbonyl intermediates are ultimately turned into desired quinoxalines **1a** and **1c** respectively, via condensations with *o*-PDA. In the presence of a minimal amount of alkali, the breakage of sugars preferentially occurs at C3–C4 linkage, achieved through slanting the aldose-ketose equilibrium towards ketose [35,36,43], resulting in a marked enhancement in the selectivity of **1b**.

The proposed reaction pathways were further supported by density functional theory (DFT) calculations. The transformation of glucose to product **1b** mainly consists of three main reaction stages (Figure 3 and Figure S20): (1) tautomerization of glucose to fructose; (2) Retro-Aldol C–C cleavage of fructose to C_3 compounds; (3) formation of **1b** via condensation of PA with *o*-PDA.

For reaction stage 1, two-type mechanisms were considered [40,44], i.e., the consecutive keto-enol tautomerism (Figure 3A) and 1,2-hydride transfer (Figure S21). The keto-enol tautomerism occurs via proton transfers between glucose and *o*-PDA, in which an enediol intermediate **14** is first formed (TS1) and then converted to fructose (TS2) with respective activation Gibbs free energies ($\Delta G^{\neq}$) of 93.6 and 54.8 kJ mol^{-1}. In contrast, *o*-PDA facilitated isomerization of glucose via 1,2-hydride shift mechanism produces fructose in single step with a $\Delta G^{\neq}$ of 124.3 kJ mol^{-1}. Thus, the keto-enol tautomerism is more competitive than 1,2-hydride shift for isomerization of glucose to fructose.

The stage 2 for fragmentation of fructose to C_3 intermediates is composed of several elementary reaction steps (Figure 3B). The activation of fructose starts by a nucleophilic attack of amino group of *o*-PDA to the carbonyl of fructose (TS3, $\Delta G^{\neq}$ = 147.4 kJ mol^{-1}), which forms a hemiaminal intermediate **15** and then dehydrates into an iminium species **16** (TS4, $\Delta G^{\neq}$ = 127.7 kJ mol^{-1}). Such an iminium species acts as the precursor for C–C cleavage, which is fragmented into GCA and an enamine intermediate **17** (TS5, $\Delta G^{\neq}$ = 47.4 kJ mol^{-1}). The computed retro-aldol reaction pathway is consistent with a previously proposed mechanism scheme for catalytic reductive aminolysis of reducing sugars [30]. In addition, the effect of water solvents on the retro-aldol reaction was also considered [44]. It was found that water solvent can strongly promote the proton transfers between fructose and *o*-PDA, resulting in a $\Delta G^{\neq}$ of only 51.5 kJ mol^{-1} (TS3'-4H_2O). The $\Delta G^{\neq}$ for the further dehydration of hemiaminal intermediate (TS4'-4H_2O) could also decrease to 118.5 kJ mol^{-1}. Furthermore, the presence of base (e.g., KOH) in the retro-aldol reaction of fructose was found to be able to strongly stabilize the iminium species (Figure S22), showing a promotion effect on the fragmentation of fructose into C_3 compounds, which is in line with the experimental results that increased yields of product **1b** were obtained in the presence of a base. The formed enamine intermediate **17** can be converted to an imine species, which then releases *o*-PDA to produce DHA. The isomerization between C_3 intermediates, i.e., GCA and DHA, occurs via a similar keto-enol tautomerism mechanism as for glucose and

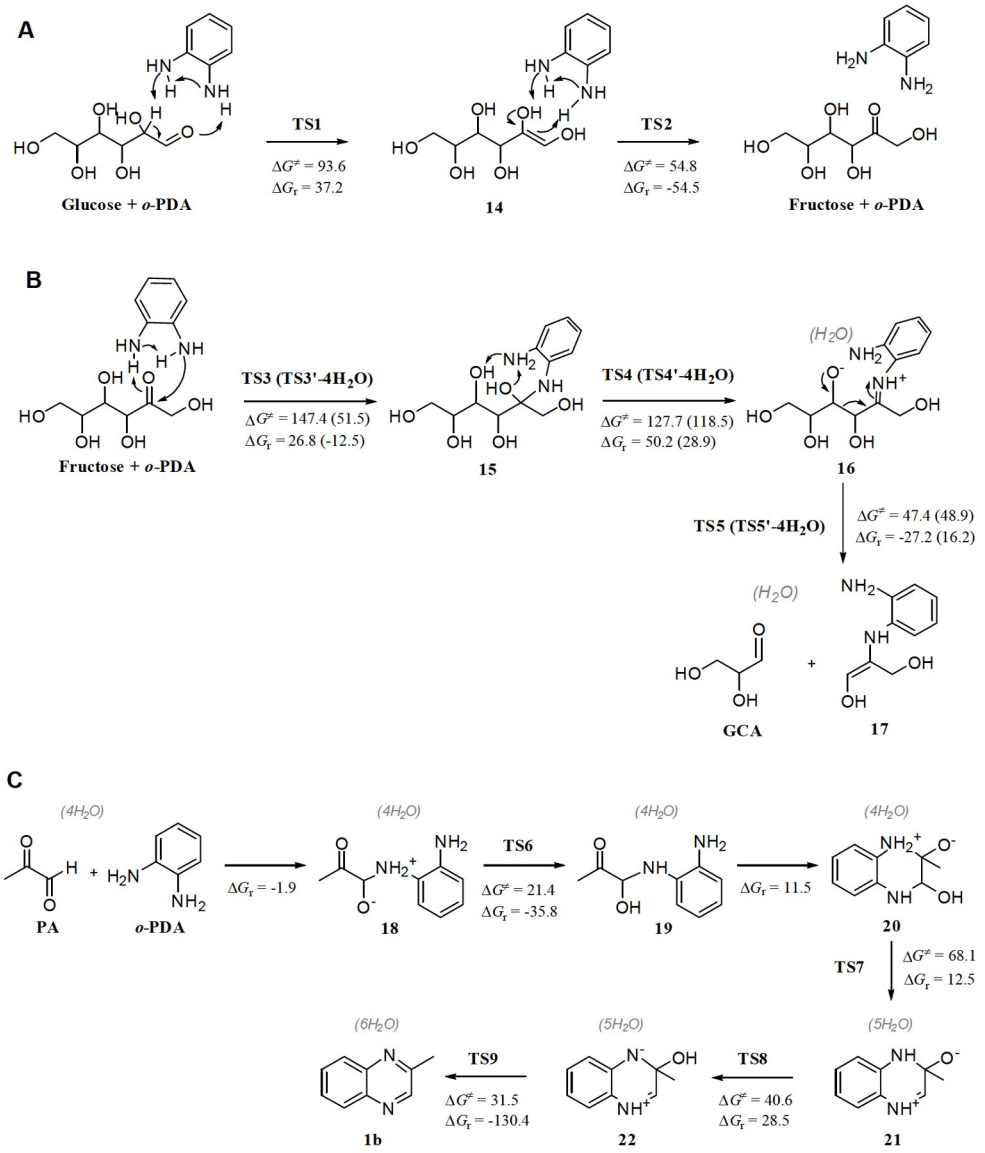

Figure 3 DFT calculations for the reaction pathways. (A) *o*-PDA facilitated isomerization of glucose to fructose via an enediol intermediate. (B) *o*-PDA facilitated retro-aldol cleavage of fructose to C_3 intermediates. (C) Condensation of PA and *o*-PDA to produce **1b** via sequential dehydrations. Activation and reaction Gibbs free energies ($\Delta G^{\neq}$ and ΔG_r) are given in kJ mol^{-1}. The structural illustrations of transition states are displayed in Figure S20.

fructose. The further dehydration of GCA produces PA (Figure S23). DFT calculations show that direct dehydration of GCA via intramolecular hydride shift is highly energy-demanding with a $\Delta G^{\neq}$ of 240.5 kJ mol^{-1} (Figure S23A), while the dehydration route promoted by *o*-PDA and explicit water molecules [44,45] requires a maximum $\Delta G^{\neq}$ of only 95.2 kJ mol^{-1} (Figure S23B), suggesting the dehydration of GCA to PA should not limit the reaction rate under employed reaction conditions.

For reaction stage 3 (Figure 3C), the reaction of PA with *o*-PDA first forms hemiaminal **19**, in which the dehydration from the hydroxy group and the proton of NH moiety requires a high $\Delta G^{\neq}$ of 119.4 kJ mol^{-1} (Figure S24). The presence of explicit water molecules is able to facilitate the proton transfers in this reaction

[44], which is similar to the reaction of fructose and *o*-PDA in stage 2. The preorganization of water molecules around the reaction center between PA and *o*-PDA leads to the formation of C–N bond between the carbonyl and amino groups, forming an intramolecular charge-separated intermediate **18** with oxygen anion and protonated amino group. Such an intermediate then proceeds proton transfer assisted by water to form intermediate **19** with a $\Delta G^{\neq}$ of 21.4 kJ mol^{-1} (TS6). The reorientation of **19** with C–N bond formation between another pair of carbonyl and amino groups generates the heterocyclic intermediate **20**, in which the positively-charged amino provides a proton to dehydrate with the hydroxy group (TS7, $\Delta G^{\neq}$ = 68.1 kJ mol^{-1}). The first dehydration step yields also an intramolecular charge-separated intermediate **21**, which proceeds hydroxy group formation from oxygen anion (TS8, $\Delta G^{\neq}$ = 40.6 kJ mol^{-1}) and then second dehydration (TS9, $\Delta G^{\neq}$ = 31.5 kJ mol^{-1}). The conversion of PA and *o*-PDA to **1b** involves crucial dehydration steps in which a protonated nitrogen provides proton to react with a hydroxy group (TS7 and TS9).

Based on the DFT calculation results, the retro-aldol reaction of fructose to C_3 intermediates is believed to be the rate-determining step in the transformation of glucose to product **1b**. This is in line with the obtained experimental results from using different sugars and their derived intermediates as the feedstocks for production of quinoxalines (Table 1, entries 12–16), and also consistent with the previous findings in the transformation of glucose to other C_3-based products [29,44].

Exploration of reaction application and integrated synthesis processes

The applicability of this reaction to other 2-methylquinoxalines of interest in pharmaceutical chemistry was encouraging. As shown in Figure 2G, 2,6,7-trimethylquinoxaline (**2b**), 6,7-difluoro-2-methylquinoxaline (**3b**), and 6,7-dichloro-2-methylquinoxaline (**4b**) were produced from corresponding disubstituted aryl-1,2-diamines with yields of 70%, 58%, and 47%, respectively. In addition, 4-substituted *o*-PDA afforded products, including **5b**, **6b**, and **7b**, which were produced in a form as a mixture of two isomers, in combined yields of 66%, 71%, and 60%, respectively. All above-mentioned 2-methylquinoxalines present as key structural scaffolds or building blocks in a variety of important bioactive compounds **8**–**13** for multifarious treatment purposes. For instances, compound **8** with **2b** moiety and **9** derived from **3b** show trypanocidal and antifungal activity, respectively [46,47]. Target **10** prepared from **4b** can be used as a glucagon receptor antagonist [48] and **12** synthesized from **6b** functions as an androgen receptor antagonist for treating prostate cancer [49]. Targets **11** and **13** derived from **5b** and **7b** respectively, possess antimalarial and antitubercular activity, respectively [50,51].

The promising results prompted us to conceive integrated processes compatible to practical reactor technology for manufacture of quinoxalines (Figure 4). Both batch and continuous-flow processes were exemplified. For batch processing, the reaction of glucose with *o*-PDA was conducted in a stirred high-pressure reactor in water at 180ºC under N_2. Upon the completion of the reaction, ethyl acetate (EA), a recommended green solvent [52], was used to extract produced quinoxalines from the aqueous phase. The aqueous reaction mixture was subjected to liquid-liquid extraction with EA by three times (V_{EA}/V_{water}=1:2) to transfer most of products **1a**–**1c** (⩾98%) and unreacted *o*-PDA (~91%, Figure S18) into organic layer. After EA solvent recycling via evaporation, the remaining mixture of products and *o*-PDA further underwent purification process, like distillation, to afford desired quinoxalines. The retrieved *o*-PDA as well as the aqueous effluent from the extractor can be reinserted into the reactor for reuse, therefore the required loading

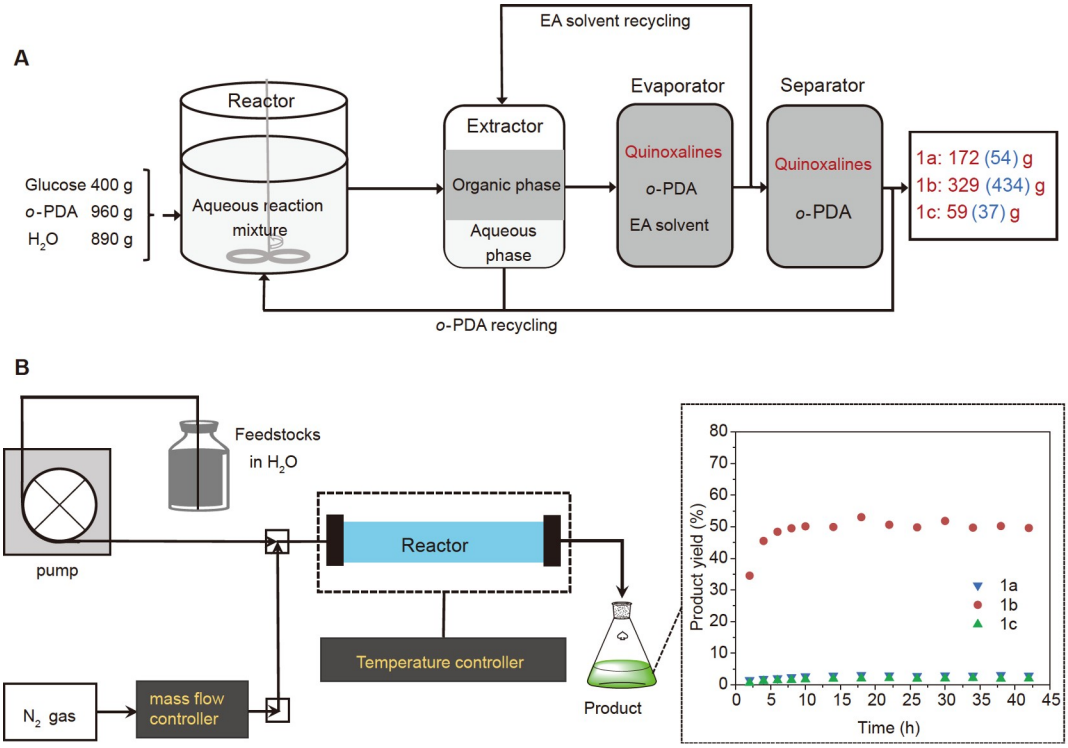

Figure 4 Reaction process schemes for manufacturing quinoxalines. (A) Batch processing. Indicative quantities of feedstocks, product and solvent are based on exemplary 400-g glucose input process, extrapolated from small-scale batch reaction. The results based on processes without base (values in red) and with 37 g of KOH (values in blue in parentheses) are provided respectively. (B) Continuous-flow processing.

of fresh *o*-PDA for next run can be reduced by nearly half. The reaction was verified by five consecutive runs in recycled aqueous medium, furnishing desired quinoxalines with comparable outcomes (Figure S25). It should be noted that although more amounts of KOH are needed to maintain the high yield of **1b** in the recycling experiments, the pH of the resulted solution is still close to a value of 7 due to the fact that roughly equivalent amounts of acidic byproducts are formed accordingly, indicating the extra addition of base in the recycling reactions would not add environmental burden. In the continuous-flow processing, **1b** yield of ~50% (~100% yield on mole basis) was stably maintained over 42 h at 3 mL h^{-1} flow rate, although the obtained yield showed slightly lower than that of batch process (Figure 4B).

Benefiting from the high efficiency (up to 82% overall yield), a minimal number of unit operations and the use of water as solvent in the transformation of sugar to quinoxalines, a rather low *E*-factor (~0.4) is achieved for this proposed reaction-based process when taking aryl-1,2-diamine recyclability into account in a small-scale batch reaction (SM). The value is much lower than 5–50 from traditional fine chemicals synthesis (Table S7).

Sustainability and economic analyses

On the basis of the experimental results, we performed a life-cycle assessment (LCA) for the production of quinoxalines. Our proposed approach showed reduced environmental footprints (Figure 5A and Table S8), as evidenced by the lower global warming potentials (GWPs) for manufacturing quinoxalines (15.5–16.9 kg of

CO_2-equivalent per kilogram of quinoxalines) when compared with the conventional petroleum-based process (21.9 kg of CO_2-equivalent per kilogram of quinoxalines). Different source of glucose and the addition of a base in our proposed production processes show minor impacts on GWPs. For instances, the use of glucose obtained from wood biomass residue shows 0.5 kg of CO_2-equivalent lower GWPs than using maize-derived glucose (Table S8). The addition of KOH in the process results in a ~1.0 kg of CO_2-equivalent increase in GWPs (Table S8). Although *o*-PDA, obtained from non-renewable fossil oil via a well-established chemical process, accounts for a large contribution of CO_2 footprint for manufacturing of quinoxalines via our approach, the overall production processes by incorporating renewable glucose could still reduce CO_2 release by nearly 30% when compared with the current complete petroleum-based route, indicating that our approach has an obvious advantage in terms of environmental impact.

In addition to the sustainability analysis, we designed a process model to perform a techno-economic analysis. The economic analysis was based on annual production of 100 t of bio-quinoxalines (**1a**–**1c**), a lower-than-average scale for petroleum-based quinoxalines (**1a**–**1c**) production in China. Among the different process units, equipment investment accounts for the highest contributor toward capital expenditures (Table S10). The production costs of quinoxalines via our proposed processes with and without KOH additive were evaluated to be 288 and 221 \$ kg^{-1}, respectively, which are lower than the market prices of quinoxalines (291–303 \$ kg^{-1}), suggesting that the proposed bio-production process is profitable (Figure 5B). This results in an internal rate of return of 16.5% and a payout time of ~6 years for a plant with a lifetime of 8 years (Table S10). Although the addition of a base in the process could lead to an increased production of **1b**, it in overall increases the cost for producing quinoxalines.

DISCUSSION

A novel sustainable strategy for efficient production of bio-based quinoxalines directly from renewable carbohydrates is presented. This carbohydrate-to-quinoxalines transformation could be spontaneously

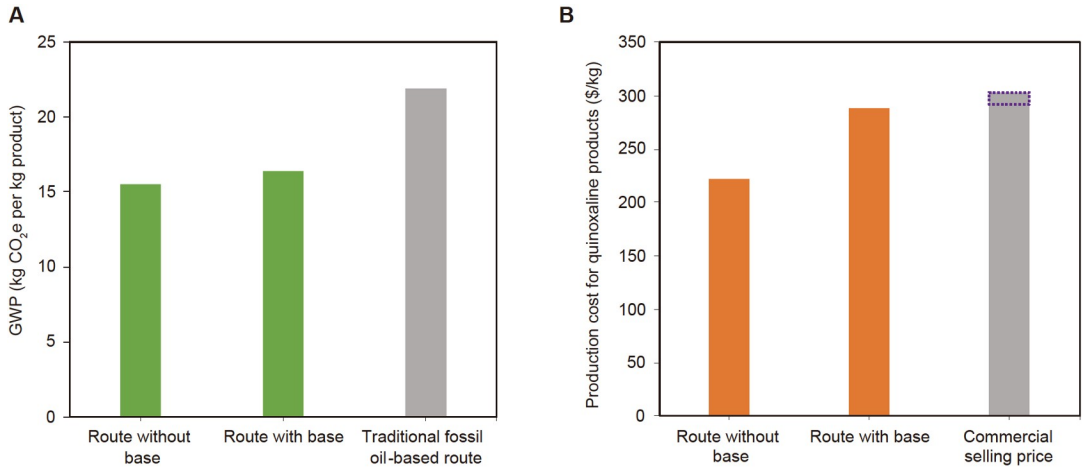

Figure 5 Sustainability and economic analyses. (A) Comparison between the sustainability of our proposed routes and the conventional petroleum-based route for manufacturing quinoxaline products. (B) Comparison between the production cost of quinoxaline products via the proposed routes and their commercial selling prices. The dashed line indicates the variation range of market selling price of quinoxalines (**1a**–**1c**) based on different product compositions.

achieved in the presence of aryl-1,2-diamines and generate water as the solely theoretical byproduct, affording quinoxalines with up to 82% overall yield. In the presence of minimal alkali, the percentage of 2-methylquinoxalines in total formed quinoxalines could reach up to 94%. The crucial functions of aryl-1,2-diamine for this transformation was identified by experiments and DFT simulations. It can not only spontaneously recognize carbohydrate substrate via interacting with its carbonyl group and improve its fragmentation into small 1,2-dicarbonyl intermediates (e.g., PA) by two orders of magnitude via an enzyme-like manner, but also rapidly trap these *in-situ* generated reactive intermediates for final formation of quinoxalines, therefore considerably inhibiting unwanted side reactions and maximizing the reaction efficiency. The strategy is applicable to diverse sugars as well as various aryl-1,2-diamines, and verified by both batch and continuous-flow processes. Furthermore, sustainability and techno-economic analyses indicate that the proposed route for production of quinoxalines show significantly reduced environmental impact and production costs (decrease by ~30%) in contrast to the current petroleum-based routes. Therefore, the work reported here may open a brand-new way for sustainable manufacture of high-value quinoxalines from largely abundant lignocellulosic resources, and pave the way for more innovative production of bio-based commodity chemicals in the future.

MATERIALS AND METHODS

The typical procedure for batch reaction

The experimental reactions were performed in a stainless steel and high pressure autoclave reactor (20 mL), equipped with a magnetic stirrer. For typical runs, 90 mg (0.5 mmol) of glucose, 216 mg (2 mmol) of *o*-PDA, and 20 mL of H_2O were loaded into an autoclave reactor. The reactor was purged with N_2 for three times to remove the air and charged with N_2 to make sure that the pressure was slightly higher than the vapor pressure of water at the reaction temperature (the initial pressure of N_2 was usually set around 2 MPa at room temperature). The autoclave reactor was heated to desired temperature for a specific time under continuous stirring. After the reaction, the reactor was removed from the heating and rapidly cooled down in an ice bath. The product mixture was then sampled for further analysis.

The typical procedure for continuous-flow reaction

A quartz column (ϕ 8 mm × 200 mm) was packed with 0.4 mm quartz beads (8.0 g) and preheated to 180ºC. To the column, feedstocks including glucose (1.80 g L^{-1}), *o*-PDA (4.32 g L^{-1}) and KOH (0.49 g L^{-1}) in H_2O were fed using a pump (3 mL h^{-1}), and inert N_2 gas was introduced simultaneously using mass flow controller (10 mL min^{-1}) by down flow. The aqueous solution of feedstocks was flowing through the reactor with the short packed-bed column. The flow system was left to stabilize for 1 h, and then the aqueous effluent was collected for analysis.

Conversion and yield calculations

The conversion of carbohydrates and their derived feedstocks was calculated based on carbon by using the

following equation:

$$\text{Conversion} = \frac{\text{mass}_{\text{initial carbohydrate}} - \text{mass}_{\text{remaining carbohydrate after reacion}}}{\text{mass}_{\text{initial carbohydrate}}} \times 100\%$$

The product yield, given in C%, represents the fraction of carbon originating from the carbohydrate or its derived feedstocks that is found in the product. The yields of all products were calculated based on carbon mass by using the following equation:

$$\text{Yield} = \frac{\text{mass}_{\text{carbon from carbohydrate in product}}}{\text{mass}_{\text{carbon in carbohydrate}}} \times 100\%$$

Computational methods

All DFT calculations were performed using the standard methods implemented in Gaussian 16 C.01 program. Geometry optimizations were performed using M06-2X functional with a basis set 6-311+G(2df,2p) for all atoms. Grimme's D3 dispersion scheme was used to describe the van der Waals interactions. Solvent effect was accounted for during the geometry optimization by SMD model with the standard parameters for water solvent as implemented in Gaussian program. The nature of optimized stationary points was evaluated from normal-mode vibrational analysis. All structures corresponding to local minima showed no imaginary frequencies while transition state (TS) structures exhibited a single imaginary frequency corresponding to the eigenvector along the reaction path. Intrinsic reaction coordinate (IRC) approach was employed to confirm the connectivity between the transition states and the corresponding minima. The activation and reaction Gibbs free energies ($\Delta G^{\neq}$ and ΔG_{r}) reported in the manuscript were computed with thermal corrections from the results of the normal-mode analysis (298.15 K and 1 atm).

Life-cycle assessment

The environmental impacts, indicated as global warming potential (GWP), from fossil oil-based quinoxalines were considered as benchmark to evaluate and compare environmental effectiveness of bio-quinoxalines production via our proposed strategy. The unit-specific inventory of production of quinoxalines from sugar and *o*-PDA is shown in Table S8. Characterization data is extracted from the Ecoinvent and USLCI databases and characterized for lifecycle impact assessment using the ReCiPe2016 midpoint and endpoint method in SimaPro. The GWPs of proposed processes for manufacturing quinoxalines with and without KOH additive were evaluated, respectively. In addition, glucose obtained from different biomass resources, including woody biomass residue and maize, was evaluated for GWP of the proposed approach.

Techno-economic analysis

To demonstrate techno-economic feasibility of the proposed processes for production of quinoxalines from sugar and *o*-PDA, we calculated the production cost for quinoxaline products synthesized via our proposed strategy, and then compared it with the current market selling price of the product. Base on the developed model and the reasonable economic assumptions, capital expense for production of quinoxalines via our

proposed strategy was calculated and shown in Table S10. Capital cost is the cost to build new facilities. In general, this is the cost for developing or providing non-consumable parts for an installation of plant. For the designed plant, the total capital cost was calculated at around 140 M$. The relatively high capital cost is related to reactor equipment and indirect cost, which includes engineering, construction, legal and contractor fees and project contingency. The techno-economic analyses of the proposed production processes with and without KOH additive were conducted.

Data availability

The original data are available from corresponding authors upon reasonable request.

Acknowledgements

The authors acknowledge the discussion with Dr. Xiaodan Wu for the LC-MS measurement of samples, and also appreciate the help from Luling Wu for NMR measurements.

Funding

This work was supported by the National Natural Science Foundation of China (21932006) and the China Postdoctoral Science Foundation (2019M652058).

Author contributions

F.Y. performed the experiments. F.Y. and F.S.X. conceived the idea, analyzed the data, and wrote the paper. C.L. performed the DFT calculations. F.T., Y.H.L., and Y.P.L. conducted the techno-economic and life-cycle assessment. L.W. participated in data analysis and provided the helpful discussion.

Conflict of interest

A patent application (CN2021105353207) that covers this sustainable synthetic strategy is pending.

Supplementary information

The supporting information is available online at https://doi.org/10.1360/nso/20230019. The supporting materials are published as submitted, without typesetting or editing. The responsibility for scientific accuracy and content remains entirely with the authors.

References

1 Koutinas AA, Du C, Wang RH *et al*. Production of chemicals from biomass. In: Clark J, Deswarte F (eds.). *Introduction to Chemicals from Biomass*. Chichester, UK: John Wiley & Sons, Ltd., 2008. 77–101.

2 Sheldon RA. Green and sustainable manufacture of chemicals from biomass: State of the art. *Green Chem* 2014; **16**: 950–963.

3 Anastas PT, Zimmerman JB. The periodic table of the elements of green and sustainable chemistry. *Green Chem* 2019; **21**: 6545–6566.

4 Wu X, Luo N, Xie S, *et al.* Photocatalytic transformations of lignocellulosic biomass into chemicals. *Chem Soc Rev* 2020; **49**: 6198–6223.

5 Luterbacher JS, Martin Alonso D, Dumesic JA. Targeted chemical upgrading of lignocellulosic biomass to platform molecules. *Green Chem* 2014; **16**: 4816–4838.

6 Rinaldi R, Schuth F. Acid hydrolysis of cellulose as the entry point into biorefinery schemes. *ChemSusChem* 2009; **2**:

1096–1107.

7 Xia Q, Chen Z, Shao Y, *et al.* Direct hydrodeoxygenation of raw woody biomass into liquid alkanes. *Nat Commun* 2016; **7**: 11162.

8 Zhang T. Taking on all of the biomass for conversion. *Science* 2020; **367**: 1305–1306.

9 Liao Y, Koelewijn SF, Van den Bossche G, *et al.* A sustainable wood biorefinery for low-carbon footprint chemicals production. *Science* 2020; **367**: 1385–1390.

10 Tuck CO, Pérez E, Horváth IT, *et al.* Valorization of biomass: Deriving more value from waste. *Science* 2012; **337**: 695–699.

11 Huang Z, Luo N, Zhang C, *et al.* Radical generation and fate control for photocatalytic biomass conversion. *Nat Rev Chem* 2022; **6**: 197–214.

12 Queneau Y, Han B. Biomass: Renewable carbon resource for chemical and energy industry. *Innovation* 2022; **3**: 100184.

13 Chen X, Yang H, Hülsey MJ, *et al.* One-step synthesis of *N*-heterocyclic compounds from carbohydrates over tungsten-based catalysts. *ACS Sustain Chem Eng* 2017; **5**: 11096–11104.

14 Ren T, Qi W, He Z, *et al.* One-pot production of phenazine from lignin-derived catechol. *Green Chem* 2022; **24**: 1224–1230.

15 Yu F, Darcel C, Fischmeister C. Single-step sustainable production of hydroxy-functionalized 2-imidazolines from carbohydrates. *ChemSusChem* 2022; **15**: 5–9.

16 Katoh A, Yoshida T, Ohkanda J. Synthesis of quinoxaline derivatives bearing the styryl and phenylethynyl groups and application to a fluorescence derivatization reagent. *Heterocycles* 2000; **52**: 911–920.

17 Pereira JA, Pessoa AM, Cordeiro MNDS, *et al.* Quinoxaline, its derivatives and applications: A state of the art review. *Eur J Medicinal Chem* 2015; **97**: 664–672.

18 Cheeseman GWH, Cookson RF. Condensed pyrazines. In: Weissberger A, Taylor EC (eds.). *Chemistry of Heterocyclic Compounds*. Vol 35. New York: John Wiley & Sons Ltd., 1979. 1–809.

19 Zviely M. Aroma chemicals II: Heterocycles. In: Rowe DJ (ed.). *Chemistry and Technology of Flavors and Fragrances*. Oxford, UK: Blackwell Publishing Ltd., 2005. 85–115.

20 Singh DP, Deivedi SK, Hashim SR, *et al.* Synthesis and antimicrobial activity of some new quinoxaline derivatives. *Pharmaceuticals* 2010; **3**: 2416–2425.

21 Kim YB, Kim YH, Park JY, *et al.* Synthesis and biological activity of new quinoxaline antibiotics of echinomycin analogues. *Bioorg Med Chem Lett* 2004; **14**: 541–544.

22 Baer H, Bergamo M, Forlin A, *et al*. Propylene oxide. In: Gerhartz W (ed.). *Ullmann's Encyclopedia of Industrial Chemistry*. Weinheim, Germany: Wiley-VCH Verlag GmbH & Co. KGaA, 2012. 1–29.

23 Sullivan CJ, Kuenz A, Vorlop K-D. Propanediols. In: Gerhartz W (ed.). *Ullmann's Encyclopedia of Industrial Chemistry*. Weinheim, Germany: Wiley-VCH Verlag GmbH & Co. KGaA, 2018, 1–15.

24 Mao J, Deng M, Chen L, *et al.* Novel microfibrous-structured silver catalyst for high efficiency gas-phase oxidation of alcohols. *AIChE J* 2010; **56**: 1545–1556.

25 Weber M, Pompetzki W, Bonmann R, et al. Acetone. In: Gerhartz W (ed.). *Ullmann's Encyclopedia of Industrial Chemistry*. Vol 207. Weinheim, Germany: Wiley-VCH Verlag GmbH & Co. KGaA, 2014. 1–19.

26 Riley HL, Morley JF, Friend NAC. 255. Selenium dioxide, a new oxidising agent. Part I. Its reaction with aldehydes and ketones. *J Chem Soc* 1932: 1875–1883.

27 Holm MS, Saravanamurugan S, Taarning E. Conversion of sugars to lactic acid derivatives using heterogeneous zeotype catalysts. *Science* 2010; **328**: 602–605.

28 Shi N, Liu Q, Ju R, *et al.* Condensation of α-carbonyl aldehydes leads to the formation of solid humins during the hydrothermal degradation of carbohydrates. *ACS Omega* 2019; **4**: 7330–7343.

29 Pelckmans M, Vermandel W, Van Waes F, *et al.* Low-temperature reductive aminolysis of carbohydrates to diamines and aminoalcohols by heterogeneous catalysis. *Angew Chem Int Ed* 2017; **56**: 14540–14544.

30 Pelckmans M, Mihaylov T, Faveere W, *et al.* Catalytic reductive aminolysis of reducing sugars: elucidation of reaction

mechanism. *ACS Catal* 2018; **8**: 4201–4212.

31 Deng W, Wang P, Wang B, *et al.* Transformation of cellulose and related carbohydrates into lactic acid with bifunctional Al(^{III})-Sn(^{II}) catalysts. *Green Chem* 2018; **20**: 735–744.

32 Hodge JE. Dehydrated foods, chemistry of browning reactions in model systems. *J Agric Food Chem* 1953; **1**: 928–943.

33 Nursten H. The chemistry of nonenzymic browning. In: Nursten H (ed.). *The Maillard Reaction*. Vol 54. Cambridge: Royal Society of Chemistry, 2005. 5–30.

34 Kroh LW. Caramelisation in food and beverages. *Food Chem* 1994; **51**: 373–379.

35 Esposito D, Antonietti M. Chemical conversion of sugars to lactic acid by alkaline hydrothermal processes. *ChemSusChem* 2013; **6**: 989–992.

36 Tolborg S, Sádaba I, Osmundsen CM, *et al.* Tin-containing silicates: Alkali salts improve methyl lactate yield from sugars. *ChemSusChem* 2015; **8**: 613–617.

37 Yu F, Xiao FS. Room-temperature and ambient-pressure conversion of renewable carbohydrates to value-added aromatic *N*-heterocycles under ultrasonic irradiation conditions. *Green Chem* 2023; **25**: 1023–1031.

38 Orazov M, Davis ME. Tandem catalysis for the production of alkyl lactates from ketohexoses at moderate temperatures. *Proc Natl Acad Sci USA* 2015; **112**: 11777–11782.

39 Angyal SJ. The Lobry de Bruyn-Alberda van Ekenstein transformation and related reactions. In: Stütz AE (ed.). *Glycoscience*. Vol 215. Berlin: Springer, 2001. 1–14.

40 Assary RS, Curtiss LA. Comparison of sugar molecule decomposition through glucose and fructose: A high-level quantum chemical study. *Energy Fuels* 2012; **26**: 1344–1352.

41 Huyghues-Despointes A, Yaylayan VA. Retro-aldol and redox reactions of amadori compounds: Mechanistic studies with variously labeled D-[13C]glucose. *J Agric Food Chem* 1996; **44**: 672–681.

42 Cha J, Debnath T, Lee KG. Analysis of α-dicarbonyl compounds and volatiles formed in Maillard reaction model systems. *Sci Rep* 2019; **9**: 5325.

43 Liu C, Carraher JM, Swedberg JL, *et al.* Selective base-catalyzed isomerization of glucose to fructose. *ACS Catal* 2014; **4**: 4295–4298.

44 Wang Y, Deng W, Wang B, *et al.* Chemical synthesis of lactic acid from cellulose catalysed by lead(II) ions in water. *Nat Commun* 2013; **4**: 2141.

45 Xu S, Tian Q, Xiao Y, *et al.* Regulating the competitive reaction pathway in glycerol conversion to lactic acid/glycolic acid selectively. *J Catal* 2022; **413**: 407–416.

46 Estevez Y, Quiliano M, Burguete A, *et al.* Trypanocidal properties, structure-activity relationship and computational studies of quinoxaline 1,4-di-*N*-oxide derivatives. *Exp Parasitology* 2011; **127**: 745–751.

47 Carta A, Loriga M, Paglietti G, *et al.* Synthesis, anti-mycobacterial, anti-trichomonas and anti-candida *in vitro* activities of 2-substituted-6,7-difluoro-3-methylquinoxaline 1,4-dioxides. *Eur J Med Chem* 2004; **39**: 195–203.

48 Collins JL, Dambek PJ, Goldstein SW, *et al.* CP-99,711: A non-peptide glucagon receptor antagonist. *Bioorg Med Chem Lett* 1992; **2**: 915–918.

49 Patil SN, Sarma BV. Androgen receptor antagonists. Patent US2019/016176, 2019.

50 Zarranz B, Jaso A, Lima LM *et al*. Antiplasmodial activity of 3-trifluoromethyl-2-carbonylquinoxaline di-*N*-oxide derivatives. *Braz J Pharm Sci* 2006; **42**: 357–361.

51 Villar R, Vicente E, Solano B, *et al. In vitro* and *in vivo* antimycobacterial activities of ketone and amide derivatives of quinoxaline 1,4-di-*N*-oxide. *J Antimicrob Chemother* 2008; **62**: 547–554.

52 Prat D, Wells A, Hayler J, *et al.* CHEM21 selection guide of classical- and less classical-solvents. *Green Chem* 2015; **18**: 288–296.